Published in final edited form as:
Dalton Trans. 2013 October 1; 42(41): . doi:10.1039/c3dt50767j.

Acid-base and Electrochemical Properties of Manganese *meso*(*ortho*- and *meta*-*N*-ethylpyridyl)porphyrins: Voltammetric and Chronocoulometric Study of Protolytic and Redox Equilibria†

Tin Weitner[a,*,‡], **Ivan Kos**[a], **Zoran Mandić**[b], **Ines Batinić-Haberle**[c], and **Mladen Biruš**[a]

[a]University of Zagreb, Faculty of Pharmacy and Biochemistry, Ante Kovačića 1, Zagreb 10000, Croatia

[b]University of Zagreb, Faculty of Chemical Engineering and Technology, Marulićev trg 19, Zagreb 10000, Croatia

[c]Duke University Medical Center, Department of Radiation Oncology, Durham, NC 27710, USA

Abstract

A growing interest in redox-active compounds as therapeutics for oxidative stress-related diseases led to the design of metalloporphyrins as some of the most potent functional SOD-mimics. Herein we report the detailed electrochemical study of the protolytic and redox equilibria of manganese *ortho* and *meta* substituted *N*-ethylpyridyl porphyrins (MnPs), MnTE-2-PyP^{5+} and MnTE-3-PyP^{5+}, in aqueous solutions. Electrochemical parameters of redox processes for all experimentally available species have been determined, as well as their diffusion coefficients and estimated sizes of aqueous cavities. The results indicate that possible change of the intracellular acidity cannot affect the antioxidant activity of MnPs *in vivo*, since no change in the $E^{0'}_{app}$ ($Mn^{III}P/Mn^{II}P$) values was observed below pH 10. Furthermore, the results confirm that both of these MnPs can be efficient redox scavengers of peroxynitrite ($ONOO^-$), another major damaging species *in vivo*. This can occur by either the single-electron reduction or the two-electron reduction of $ONOO^-$, involving either the $Mn^{IV}P/Mn^{III}P$ redox couple or $Mn^{IV}P/Mn^{II}P$ redox couple. In addition to $k_{red}(ONOO^-)$ reported previously, the thermodynamic parameters calculated herein imply a strong and identical driving force for the reaction of both *ortho* and *meta* isomeric MnPs with $ONOO^-$. An enlargement of both $Mn^{III}P$ complexes upon increase of the solution pH was also observed and attributed to the reduction of positive charge on the central ion caused by the deprotonation of the axial water molecules. This expansion of aqueous cavities suggests the formation of a solvent cage and the increased lipophilicity of $Mn^{III}P$ complexes caused by increased electron density on the Mn ion.

INTRODUCTION

In recent years there has been considerable interest in the research of cellular oxidative stress which is a condition of imbalance between the metabolic production of reactive oxygen and nitrogen species (ROS and RNS, respectively) causing damage to cellular components (lipids, proteins and nucleic acids) and the cellular ability to scavenge the

†Dedicated to the memory of Ivan Kos, our dear friend and colleague.

*Corresponding author: Tin Weitner, Ph.D., Faculty of Pharmacy and Biochemistry, Ante Kovačića 1, Zagreb 10000, Croatia, phone: +385 1 4818 305, tweitner@pharma.hr.

‡Taken in part from Tin Weitner's Ph.D. thesis submitted to University of Zagreb.

reactive metabolites or repair the incurred damage. The molecular species implicated in the oxidative stress are the superoxide anion ($O_2^{\bullet-}$), peroxynitrite ($ONOO^-$), the hydroxyl radical ($OH^\bullet$), etc. A schematic representation of the reactions involved in the cellular oxidative stress is given in Figure S1. An effective cellular defence from the $O_2^{\bullet-}$ exists in the class of superoxide-dismutase enzymes (SOD). SOD-deficiency is linked to numerous pathological conditions, including diabetes, pulmonary, cardiovascular and degenerative diseases, as well as carcinogenesis.[1–3] An optimal dismuting ability of a compound is expected when the formal reduction potential is midway between the single-electron formal reduction potentials for oxygen ($E^{0\prime}$ = − 0.16 V *vs*. NHE) and superoxide ($E^{0\prime}$ = + 0.89 V *vs*. NHE),[4–5] providing a similar driving force for both half-reactions of the dismutation cycle. This is indeed the case with the SOD enzymes,[6] but also with several manganese porphyrins (MnPs) that proved to be robust redox catalysts due to their unique electronic properties and the accessibility of several oxidation states of manganese.[7–10]

A structure-activity relationship (SAR) established for MnPs, relating the metal-centred reduction potential ($E_{1/2}$) and the catalytic rate constant for the $O_2^{\bullet-}$ dismutation (log k_{cat}), led to the design of some of the most potent functional SOD-mimics described so far.[11–18] The formal reduction potential of manganese *ortho* tetrakis(*N*-ethylpyridinium-2-yl)porphyrin (MnTE-2-PyP, Figure 1a), bearing *ortho* cationic aromatic heterocyclic groups, is close to the potential of the SOD enzyme itself, which in turn results in excellent SOD-like activity, both *in vitro* and *in vivo*.[14–15, 19] Moreover, the increased lipophilicity and rotational flexibility of the more recently synthesized isomer, Mn *meta* tetrakis(*N*-ethylpyridinium-3-yl)porphyrin (MnTE-3-PyP, Figure 1b),[20] resulted in an increased cellular uptake. Considering that these compounds are able to equally efficiently dismute $O_2^{\bullet-}$ and also reduce $ONOO^-$ or $CO_3^{\bullet-}$,[21–22] their application under pathological conditions could help alleviate oxidative stress and reduce cellular damage. A reactivity scheme of MnPs in the presence of cellular reductants in aqueous solutions is given in Figure S2.[14, 22–31]

The axial coordination of the central metal ion is crucial for understanding the reactivity of MnPs. In an aqueous solution MnPs can axially coordinate water molecules, which, depending on the manganese oxidation state and pH, can deprotonate to hydroxo- and/or oxo-ligands.[33–34] We have recently proposed a scheme of the speciation of $Mn^{II–IV}$TE-2-PyP and $Mn^{II–IV}$TE-3-PyP in a broad pH range (Figure 2).[32] These equilibria can have a profound influence on the redox activity and the corresponding biological effects of metalloporphyrins, as evidenced in a recent study,[35] where the reduced electron-deficiency of the metal site in $(OH)(H_2O)$FePs *vs*. $(H_2O)_2$MnPs at physiological conditions resulted in vastly different SARs for a series of isomeric *N*-alkylpyridyl Fe and Mn porphyrins. As the scheme in Figure 2 is meant to be general, the corresponding Mn(V) species were included in order to account for the species of *N*-methylpyridyl isomers characterised in the modelling of haloperoxidases.[36–39]

Herein we report the detailed electrochemical study of the protolytic and redox equilibria of Mn(II)–(IV) porphyrins in aqueous solutions. Electrochemical parameters of redox processes for all the experimentally available species have been determined, including their diffusion coefficients and the estimated sizes of aqueous cavities. The thermodynamic parameters for the reaction of both *ortho* and *meta* isomeric Mn porphyrins with peroxynitrite have been calculated as well.

EXPERIMENTAL

Throughout the experiments, the water used was double-distilled in an all-glass apparatus and the highest purity chemicals were used. The investigated metalloporphyrins, Mn^{III}TE-2-

$PyPCl_5$ and Mn^{III}TE-3-$PyPCl_5$, were synthesized according to the published procedures.[14, 20] Stock solutions of MnPs were prepared by dissolution of solid substances in the double-distilled water. Buffers used for the working solutions were prepared from $Na_2B_4O_7 \times 10H_2O$ (Riedel-de Haën), CAPS (*N*-cyclohexyl-3-aminopropanesulfonic acid) (Sigma), NaH_2PO_4 (Merck) and $Na_2HPO_4 \times 2H_2O$ (Merck). The pH of the working solutions was adjusted by the addition of standard solutions of HCl or NaOH. The supporting electrolyte in all measurements was 0.1 M NaCl. The final concentrations of MnPs in the working solutions were determined spectrophotometrically from known molar absorbance coefficients (ε_{455} (MnTE-2-PyP) = 1.38×10^5 M^{-1} cm^{-1} and ε_{462} (MnTE-3-PyP) = 1.55×10^5 M^{-1} cm^{-1}).[9]

Cyclic voltammetry (CV) and chronocoulometry (CC) were performed in a BASi VC-5 cell under anaerobic conditions using a three-electrode CH Instruments 600D potentiostat with iR-drop compensation, on-line connected to a PC. The data were treated by CHI software v11.13. The working, reference and auxiliary electrode were a glassy carbon (GC) electrode, the Ag/AgCl standard electrode (3 M NaCl) and a platinum wire, respectively. The GC electrode was polished with an aqueous alumina slurry with particles 0.05 μm in diameter before every experiment and the electrode surface was determined to be $A = 0.085 \pm 0.010$ cm^2 by chronocoulometry of a 2 mM solution of $K_3[Fe(CN)_6]$ in 1 M aqueous KCl.[40–42] The pH of aqueous solutions was determined on a Mettler Toledo T70 titrator with Mettler DG-111-SC glass electrode calibrated with the standard buffers pH 4.00, 7.00 and 10.00. The potentials are reported *vs*. the standard hydrogen electrode (SHE, referring to the hydrogen pressure of 1 bar), unless stated differently. Electrochemical simulations were performed using DigiElch software.[43]

RESULTS

Cyclic voltammetry of MnTE-2-PyP and MnTE-3-PyP

Cyclic voltammograms of the aqueous solutions of Mn^{III}Ps recorded at various pH values and scan rates indicate two distinct electron transfer processes attributed to $Mn^{III}P/Mn^{II}P$ and $Mn^{IV}P/Mn^{III}P$ redox couples. In neutral and mildly basic media only one pH-independent current peak pair has been observed and has been attributed to $Mn^{III}P/Mn^{II}P$ electron transfer process (Figures 3 and S3). At pH values above 10 an additional fully developed current peak pair appeared at more positive potentials, corresponding to the $Mn^{IV}P/Mn^{III}P$ redox transition (Figures 3 and S3). The cathodic and anodic current peak potentials, E_{pc} and E_{pa}, of both redox processes shift toward more negative values upon increasing pH of the solution. The cathodic-anodic peak separation, $\Delta E_p = |E_{pc} - E_{pa}|$, for both redox processes increases with ν at all values of pH, indicative of a quasi-reversible single-electron transfer. Dependency of peak current, i_p, *vs.* $\nu^{1/2}$ for both redox processes (insets of Figures 4 and S4) clearly demonstrates the transition from approximately reversible electron transfer at low values of ν, to approximately irreversible electron transfer at high values of ν, also characteristic for quasi-reversible electron transfers.

Parameters of the recorded cyclic voltammograms were evaluated according to the previously published procedures.[44–45] The current peak potentials E_{pc} and E_{pa} were taken directly from the CHI software and used to calculate the half-wave potential, $E_{1/2} = (E_{pc} + E_{pa})/2$. The apparent rates of electron transfer, k^0_{app}, were estimated from the polynomial model of dependence of ΔE_p on log ψ (Figure S5), assuming that the rigidity of the porphyrin ring prevents a significant difference between the diffusion coefficients of the oxidized and the reduced species (*i.e.* $D_O \approx D_R$ and $E_{1/2} \approx E^{0'}$, according to the expression $E_{1/2} = E^{0'} + R\,T/(n\,F) \ln (D_R/D_O)^{1/2}$).[46] The parameter ψ is defined as $\psi = (D_O/D_R)^{\alpha/2}\, k^0_{app}\, (\pi\, D_O\, f\, \nu)^{-1/2}$, where D_O and D_R are the diffusion coefficients of the oxidized and the reduced species, α is the cathodic electron transfer coefficient and $f = F/(R\,T)$, whereas the

ΔE_p *vs.* log ψ couples were obtained from data published by Nicholson.[47] The obtained k^0_{app} values are the rates of the electron exchange in the condition of $E = E^{0\prime}$, *i.e.* when the rates of both reduction and oxidation reactions have the same value equal to k^0_{app}, which represents a measure of the kinetic facility of a redox couple.[48] The apparent values of the cathodic electron transfer coefficient, α_{app}, are a measure of the symmetry of the redox transfer energy barrier,[48] and were estimated by simulating the recorded voltammograms using the DigiElch software (a typical simulation is given in Figure S6). A summary of the estimated electrochemical parameters for the $Mn^{III}P/Mn^{II}P$ and $Mn^{IV}P/Mn^{III}P$ redox couples is given in Table S7.

The obtained results indicate a single-electron reduction of $Mn^{III}Ps$ in a neutral medium, according to eq. (1).

$$(H_2O)_2\,Mn^{III}TE{-}m{-}PyP^{5+}+e^- \rightleftarrows (H_2O)Mn^{II}TE{-}m{-}PyP^{4+}+H_2O \quad (1)$$

The observed pH-independence of the formal reduction potential and other electrochemical parameters of the $Mn^{III}P/Mn^{II}P$ redox couple at pH < 10 confirmed that no simultaneous protolysis occurs in the electron transfer process. As the pH value of the solution increases above 10, a negative shift of the observed formal potential can be observed and attributed to the deprotonation of an axial water molecule either at $Mn^{III}P$ or $Mn^{II}P$, or both. The cyclic voltammograms recorded at higher pH values of the solutions are the result of the existence of mixtures of various deprotonated species of $Mn^{III}P$ and $Mn^{II}P$ which behave as simple single-electron transfers whose apparent formal potentials, $E^{0\prime}_{app}$, and rates of electron transfer, k^0_{app}, are pH-dependent.[50–54] Therefore, the observed pH-dependence of voltammograms can be attributed to the protolysis equilibria depicted in Figure 2.

The redox reaction involving the $Mn^{IV}P/Mn^{III}P$ redox couple shows significant dependence on pH. This electron transfer cannot be observed in a neutral medium due to a formal potential more positive than that of water.[32] However, the formal potential of the $Mn^{IV}P/Mn^{III}P$ redox couple decreases upon the increase of the pH of the solution resulting in the increased rate of the electron transfer and the development of the well defined peak current couples (Figures 3 and S3). Such a behaviour can be attributed to a single-electron reduction accompanied by simultaneous dissociation of two protons, according to eq. (2).

$$(O)\,(H_2O)Mn^{IV}TE{-}m{-}PyP^{4+}+2H^++e^- \rightleftarrows (H_2O)_2Mn^{III}TE{-}m{-}PyP^{5+} \quad (2)$$

As the pH value of the solution increases above 10, the formal reduction potential of the $Mn^{IV}P/Mn^{III}P$ redox couple shifts negatively by approximately 120 mV per pH unit which is in excellent agreement with the Nernst equation predicting a shift of −118 mV per pH unit for a two-proton, single-electron oxidation which is thermodynamically favoured in basic media. Further increase of the pH above 12 results in a negative shift of approximately 60 mV per pH unit which is again in excellent agreement with the Nernst equation predicting a shift of −59 mV per pH unit for a single-proton, single-electron reduction given in eq. (3).

$$(O)\,(OH)Mn^{IV}TE{-}m{-}PyP^{3+}+H^++e^- \rightleftarrows (O)\,(H_2O)Mn^{III}TE{-}m{-}PyP^{3+} \quad (3)$$

Thermodynamics of electroreduction of Mn^{III}TE-2-PyP and Mn^{III}TE-3-PyP

The thermodynamic parameters of the electroreduction of $Mn^{III}P$ complexes were obtained by measuring the temperature dependence of the cyclic voltammograms of the $Mn^{III}P/Mn^{II}P$

redox couple (Figure S8). The measurements were performed in the range from 20 °C to 45 °C at pH = 7.5 where the fully protonated species of both Mn^{III}Ps and Mn^{II}Ps are dominant in the solution.[32] The response of the working electrode was measured *vs*. the Ag/AgCl reference whose temperature response was previously calibrated *vs*. the saturated calomel electrode (SCE) under the same experimental conditions. From the known temperature dependence of the SCE potential *vs*. SHE,[55] the temperature dependence of the potential of the Ag/AgCl reference *vs*. SHE was calculated to be: $E_{Ag/AgCl}$ *vs*. SHE = $-1.72381 \times 10^{-5} T^2 + 0.01013\ T - 1.29508$, $R^2 = 0.9948$ (Figure S9). It follows that the temperature dependence of the formal reduction potential ($E^{0\prime}$ *vs*. SHE) and the absolute reduction potential ($E^{0\prime}$(abs)) for the $Mn^{III}P/Mn^{II}P$ redox couple can be determined from the known temperature dependence of the potential of the Ag/AgCl reference *vs*. SHE and the values of $E_{1/2}$ obtained by cyclic voltammetry, again assuming $D_O \approx D_R$ and $E_{1/2} \approx E^{0\prime}$ (Figures 5 and S10). The absolute formal reduction potential was calculated according to eq. (4), where θ is the experimental temperature in °C and $\Delta_{\frac{1}{2}r}S^*_{H^+/H_2} = 85.2\ J\ K^{-1}\ mol^{-1}$ is the absolute entropy change of the standard hydrogen electrode reaction.[56–57] Finally, the thermodynamic parameters of electroreduction of Mn^{III}Ps were calculated as $\Delta S^{0\prime} = (n\ F\ \Delta E^{0\prime})/\Delta T$ and $\Delta H^{0\prime} = -n\ F\ E^{0\prime} - T\Delta S^{0\prime}$ and are given in Table 1.

$$E^{0'}(\mathrm{abs}) = E^{0'}\ vs.\mathrm{SHE} + 4.44 + (\theta - 25^{\circ}\mathrm{C})\frac{\Delta_{\frac{1}{2}r}S^*_{H^+/H_2}}{F} \quad (4)$$

Chronocoulometry of the electroreduction of Mn^{III}TE-2-PyP and Mn^{III}TE-3-PyP

Chronocoulometric measurements in the duration of t_{max} = 0.4 s were performed at various pH values in the same solutions and under the same conditions as the CV. The values of the first step potential, E_1, and the second step potential, E_2, were selected to be approximately 200 mV more positive and approximately 300 mV more negative than the formal potentials of the $Mn^{III}P/Mn^{II}P$ couples, respectively, as determined by the simulations of CV measurements (Table S7). Typical chronocoulograms of aqueous solutions of MnPs are shown in Figure 6. The apparent diffusion coefficients of Mn^{III}Ps, D_{app}, were calculated from the slopes, $\Delta Q/\Delta t^{1/2}$, of the background-corrected Anson plots[58–59] obtained directly from the CHI software (typical Anson plots are shown in the insets of Figure 6). Additionally, the apparent radii of aqueous cavities of Mn^{III}Ps were calculated according to the known Stokes-Einstein relation, $r_{app} = k_B\ T/(6\ \pi\ \eta\ D_{app})$, where k_B is the Boltzmann constant and $\eta = 0.899 \times 10^{-3}$ kg m^{-1} s^{-1} is the viscosity of 0.1 M aqueous solution of NaCl.[60–62] The results of chronocoulometric measurement of the electroreduction of Mn^{III}Ps are given in Table 2.

DISCUSSION

The electrochemical behaviour of 0.5 mM solutions of MnPs in the range of pH values from 7 to 13 was successfully simulated according to the scheme shown in Figure 2. The previously published values of the experimentally available deprotonation constants and formal reduction potentials $E_1{}^{0\prime}$ and $E_6{}^{0\prime}$ were used for the simulations,[32] as well as the values of α_{app} and $k^0{}_{app}$ from Table S7. The experimentally unavailable deprotonation constants were taken to be at least one pH unit beyond the studied pH range ($pK'_{a2} = 14$, $pK_{a3} = 14$, $pK_{a4} = 15$, $pK''_{a1} = 5$, $pK''_{a2} = 6$, $pK''_{a4} = 14$). These values were used for all simulations and expressions below. Other parameters used in the simulations were the reported value of the diffusion coefficient of H^+(aq), $D_{H+} = 9.3 \times 10^{-5}$ cm^2 s^{-1},[63] the electrode surface area $A = 0.085$ cm^2 and the rates of the protonation reactions estimated as $k_p = 10^{10}$ dm^3 mol^{-1} s^{-1}.[64] The results of these simulations are shown in Figures 7 and S11.

The appropriate Nernst equation for the pH-dependent apparent formal reduction potentials of the $Mn^{III}P/Mn^{II}P$ redox couple, $E^{0'}_{app}$ ($Mn^{III}P/Mn^{II}P$), at 25 °C according to the scheme shown in Figure 2 is given in eq. (5), where $E_1{}^{0'}$ is the formal reduction potential of the fully protonated species of the $Mn^{III}P/Mn^{II}P$ redox couple, and the values of f_X are given by the eqs. (6) and (7).[65]

$$E^{0'}_{app}\left(Mn^{III}P/Mn^{II}P\right)=E^{0'}_{1}-0.05916\log\frac{f_{Mn^{III}P}}{[H^+]^2 f_{Mn^{II}P}} \quad (5)$$

$$f_{Mn^{III}P}=\left[H^+\right]^4+\left[H^+\right]^3 K_{a1}+\left[H^+\right]^2 K_{a1}K_{a2}+\left[H^+\right] K_{a1}K_{a2}K_{a3}+K_{a1}K_{a2}K_{a3}K_{a4} \quad (6)$$

$$f_{Mn^{II}P}=\left[H^+\right]^2+\left[H^+\right] K'_{a1}+K'_{a1}K'_{a2} \quad (7)$$

Considering that the value of $E_4{}^{0'}$ is not experimentally accessible, the pH-dependent formal reduction potential of the $Mn^{IV}P/Mn^{III}P$ redox couples can be expressed relative to the formal reduction potential $E_6{}^{0'}$, determined by the oxidation of $Mn^{III}Ps$ with octacyanomolybdate ($E_6{}^{0'}$ = + 0.578 V *vs*. SHE and $E_6{}^{0'}$ = + 0.479 V *vs*. SHE for MnTE-2-PyP and MnTE-3-PyP, respectively).[32] Therefore, the $E^{0'}_{app}$ ($Mn^{IV}P/Mn^{III}P$) is given by eq. (8), where the values of f_X are given by eqs. (9) and (10).

$$E^{0'}_{app}\left(Mn^{IV}P/Mn^{III}P\right)=E^{0'}_{6}-0.05916\log\frac{f_{Mn^{IV}P}}{f_{Mn^{III}P}} \quad (8)$$

$$f_{Mn^{IV}P}=\frac{[H^+]^2}{K''_{a1}K''_{a2}}+\frac{[H^+]}{K''_{a2}}+1+\frac{K''_{a3}}{[H^+]}+\frac{K''_{a3}K''_{a4}}{[H^+]^2} \quad (9)$$

$$f_{Mn^{III}P}=\frac{[H^+]^2}{K_{a1}K_{a2}}+\frac{[H^+]}{K_{a2}}+1+\frac{K_{a3}}{[H^+]}+\frac{K_{a3}K_{a4}}{[H^+]^2} \quad (10)$$

The $E^{0'}_{app}$ values of the $Mn^{III}P/Mn^{II}P$ and $Mn^{IV}P/Mn^{III}P$ redox couples, simulated by eqs. (5) and (8), compare reasonably well with the previously published values determined spectrophotometrically[32] and the values presented in this paper, as shown in Figures 8 and S12 (the values of the experimentally unavailable deprotonation constants were the same as the simulations shown in Figures 7 and S11). The most significant deviation can be observed for the values of $E^{0'}_{app}$ ($Mn^{IV}P/Mn^{III}P$) determined by oxidation of $Mn^{III}P$ with octacyanomolybdate,[32] which is most likely related to the complex photolytic and hydrolytic reactions of octacyanomolybdate,[66] shifting the octacyanomolybdate(V/IV) equilibrium during spectrophotometric titrations and consequently shifting the apparent formal potential to more positive values. Shifting the values of $E_6{}^{0'}$ from ref. 32 by approximately −100 mV (Table 3) for both MnTE-2-PyP and MnTE-3-PyP yielded good simulations of CV data (Figures 8 and S12). Other small deviations from the simulated curves can be attributed to the differences in the ionic media used for the electrochemical measurements presented here and the spectrophotometric determinations of the deprotonation constants[32] (0.1 M NaCl and 2 M $NaClO_4$, respectively), because it was shown that the deprotonations of the axial water molecules exhibit a strong dependence on the ionic strength of the solution.[49]

A further deviation can be observed for the value of $E^{0'}_{app}$ ($Mn^{III}P/Mn^{II}P$) of MnTE-3-PyP determined by the reduction of $Mn^{III}P$ with ascorbate and the values determined electrochemically (Figure S12). The extent of this deviation cannot be attributed solely to the difference in ionic strength, since no proton exchange occurs upon the reduction of the $Mn^{III}P$ at pH values below 10 where the fully protonated species of $Mn^{III}P$ and $Mn^{II}P$ are dominant in the solution (*i.e.* $E^{0'}_{app}$ ($Mn^{III}P/Mn^{II}P$) = $E_1{}^{0'}$ in the scheme shown in Figure 2). However, the dehydroascorbic acid produced by the reduction of $Mn^{III}P$ is likely to decompose to some extent in this range of pH[67] (even though special care was taken to eliminate this during experiments[32]), thus shifting the ascorbate/dehydroascorbic acid equilibrium and consequently shifting the apparent formal potential of the ascorbic acid to more positive values.

Following the procedure outlined by Laviron,[54] a general expression describing the pH-dependence of k^0_{app} ($Mn^{III}P/Mn^{II}P$) for the electron transfer involving two deprotonations of the oxidized and the reduced species (six-member ladder scheme) can be derived. The expression is given in eqs. (11)–(13), where K_{a1} and K_{a2} are the deprotonation constants of the $Mn^{III}P$ species, K'_{a1} and K'_{a2} are the deprotonation constants of the $Mn^{II}P$ species, whereas $k_X{}^0$ and α_X are the heterogeneous electron exchange rates and transfer coefficients, respectively, of redox processes characterized by the formal potentials $E_1{}^{0'}$, $E_2{}^{0'}$ and $E_3{}^{0'}$ in Figure 2.

$$k^0_{app}\left(Mn^{III}P/Mn^{II}P\right)=\left[ak^0_1+k^0_2+bk^0_3\right]\left(\frac{[H^+]}{K_{a1}}+1+\frac{K_{a2}}{[H^+]}\right)^{\alpha_2-1}\left(\frac{[H^+]}{K'_{a1}}+1+\frac{K'_{a2}}{[H^+]}\right)^{-\alpha_2} \quad (11)$$

$$a=\frac{[H^+]}{K_{a1}{}^{1-\alpha_1}\,K'_{a1}{}^{\alpha_1}} \quad (12)$$

$$b=\frac{K_{a2}{}^{1-\alpha_3}\,K'_{a2}{}^{\alpha_3}}{[H^+]} \quad (13)$$

The apparent heterogeneous electron transfer rates of the $Mn^{III}P/Mn^{II}P$ couples first increase upon their deprotonation, and then decrease again upon further increase of pH. The increase of k^0_{app} for the mono-deprotonated $Mn^{III}P/Mn^{II}P$ couple is surprising, considering the reduced overall positive charge of the complex and the lower formal reduction potential, which might be indicative of a concerted proton-electron transfer.[68] The $Mn^{III}P/Mn^{II}P$ electron transfers of both complexes are characterized by the apparent cathodic transfer coefficients $\alpha_{app} < 0.5$ at all pH values, which is indicative of an asymmetric potential-energy function for the transition state, meaning that the activated complexes of both redox processes have predominantly the structure of the oxidized species because the change of the potential on the working electrode exhibits greater influence on the reduction activation energy, $\Delta G_c^{\ddagger}$.[69] This could be the result of a change of the complex geometries from an octahedral to a near square pyramidal upon the reduction of $Mn^{III}P$s, since the $Mn^{II}P$s coordinate only one axial water molecule because of an increase of the manganese ion radius.[34] Similar results were also previously reported for the n-butyl isomer of the same series, MnTnBu-2-PyP (the calculated values of $E_i{}^{0'}$ for all experimentally available species are given in Table S13, for comparison with Table 3).[49]

A general expression, similar to eq. (11), describing the pH-dependence of k^0_{app} ($Mn^{IV}P/Mn^{III}P$) in the range of pH values from 10 to 13 is given in eqs. (14)–(16), where K''_X are the deprotonation constants of the $Mn^{IV}P$ species, K_X are the deprotonation constants of the

$Mn^{III}P$ species, $k_X{}^0$ and α_X are the heterogeneous electron transfer rates and coefficients, respectively, of redox processes characterized by the formal potentials $E_5{}^{0\prime}$, $E_6{}^{0\prime}$ and $E_7{}^{0\prime}$ in Figure 2. The values of f_X are given by eqs. (9) and (10).

$$k^0_{app}\left(Mn^{IV}P/Mn^{III}P\right)=\left[ak^0_5+k^0_6+bk^0_7\right]\ f_{Mn^{IV}P}{}^{\alpha_6-1}\ f_{Mn^{III}P}{}^{-\alpha_6} \quad (14)$$

$$a=\frac{[H^+]}{K''_{a2}{}^{1-\alpha_5}\ K_{a2}{}^{\alpha_5}} \quad (15)$$

$$b=\frac{K''_{a3}{}^{1-\alpha_7}\ K_{a3}{}^{\alpha_7}}{[H^+]} \quad (16)$$

The values of $k^0{}_{app}$ observed for the $Mn^{IV}P/Mn^{III}P$ couples first begin to increase with the increase of the pH of the solution, in agreement with the redox equilibrium given by eq. (2) and the stabilization of the oxidation product upon the increase of pH. Further increase of the pH of the solution leads to a decrease of the $k^0{}_{app}$ values as the redox equilibrium given by eq. (3) becomes dominant in the solution due to the deprotonation of the MnP species. The changes in the electron transfer rates for the $Mn^{IV}P/Mn^{III}P$ couples are of similar magnitude for both isomers, but the electron transfer of the *meta* isomer is slightly more rapid, most probably due to its structural flexibility facilitating the approach of the redox-active site to the surface of the electrode.

Despite the fact that the *ortho* ethyl substitution of the pyridyl moiety in tetrakis(*N*-ethylpyridinium-2-yl)porphyrin yields somewhat bulkier porphyrin than the analogous *meta* substitution,[70] a 1-Å larger average radius of the diaqua Mn^{III}TE-3-PyP (r_{app} = 11.3 Å) relative to the diaqua Mn^{III}TE-2-PyP (r_{app} = 10.3 Å) is observed (Table 4). This could indicate that the measured radii of the complexes are actually more closely related to the distances between the central Mn(III) ion and the terminal ethyl hydrogen atoms, the distances that are expected to be larger in *meta* than *ortho* isomers. In turn one could also speculate that the complex ions are attached to the electrode surface through the axially coordinated water molecule, since the obtained radius is related to the equatorial area of each complex. A slightly higher value of the obtained diffusion coefficient of the *ortho* than *meta* MnP isomer (D_{app} = 2.35 × 10^{-6} cm^2 s^{-1} *vs.* D_{app} = 2.15 × 10^{-6} cm^2 s^{-1} at pH = 7.5, respectively) is presumably caused by a weaker hydration of the former isomer due to its increased bulkiness.

The obtained chronocoulometric results indicate an enlargement of both $Mn^{III}P$ complexes at the electrode surface (an increase of r_{app}) upon increase of the solution pH, which can be attributed to the reduction of positive charge on the central ion caused by the deprotonation of the axial water molecules. This is indicative of the expansion of their aqueous cavities in bulk aqueous medium (this model treats the solvent as a high-dielectric continuum, interacting with charges that are embedded in a spherical cavity of lower dielectric),[71–73] whereas the formation of a solvent cage causes their reduced mobility.[74] Such finding is in agreement with a previous study on the lipophilicity of MnPs, wherein the loss of a single charge on cationic MnPs upon reduction with ascorbate increases their lipophilicity (and in turn their bioavailability) up to 3 orders of magnitude.[75]

The expressions for the pH-dependence of D_{app} values of $Mn^{III}Ps$ are given in eqs. (17) and (18), where H_2A, HA^- and A^{2-} denote the protonated, mono-deprotonated and di-

deprotonated species of $Mn^{III}P$ complexes.[76] Solving the systems of these equations with known $Mn^{III}P$ deprotonation constants[32] yielded the values of D_O and r_O given in Table 4.

$$D_{app}=\frac{1}{f}\left(\left[H^+\right]^2 D_{H_2A}+\left[H^+\right] K_{a1}D_{HA^-}+K_{a1}K_{a2}D_{A^{2-}}\right) \quad (17)$$

$$f=\left[H^+\right]^2+\left[H^+\right] K_{a1}+K_{a1}K_{a2} \quad (18)$$

In conclusion, regarding the antioxidant therapeutic potential of the investigated metalloporphyrins, the results reported in this work undoubtedly demonstrate that below pH 10 there is no change in the $E^{0\prime}_{app}$ ($Mn^{III}P/Mn^{II}P$) values, indicating that possible change of the intracellular acidity cannot affect the antioxidant activity of MnPs *in vivo*. Furthermore, we have calculated the thermodynamic parameters that support the reactivity of both MnPs studied herein as efficient scavengers of peroxynitrite in a neutral aqueous medium. This reaction occurs either by the single-electron reaction involving the $Mn^{IV}P/Mn^{III}P$ redox couple (k_{red}(MnTE-2-PyP, 37 °C) = 3×10^7 M^{-1} s^{-1}), or the two-electron reaction involving the $Mn^{IV}P/Mn^{II}P$ redox couple (k_{red}(MnTE-2-PyP, 37 °C) > 10^7 M^{-1} s^{-1}).[22] In the latter case, the first step is the reduction of $Mn^{III}P$ with cellular reductants, $O_2^{\bullet-}$, or protein thiols (Figure S2). [22, 27, 29–30, 77] The corresponding formal potentials for the reduction of MnPs, $E^{0\prime}$ ($Mn^{IV}P/Mn^{III}P$) and $E^{0\prime}$ ($Mn^{IV}P/Mn^{II}P$) in a neutral aqueous medium can be calculated as 0.980 V and 0.563 V *vs.* SHE for MnTE-2-PyP and 0.993 V and 0.487 V *vs.* SHE for MnTE-3-PyP, respectively (Table S14). The related formal potentials for single-electron and two-electron reductions of $ONOO^-$ are $E^{0\prime}$ ($ONOO^-/NO_2^{\bullet}$) = 1.6V and $E^{0\prime}$ ($ONOO^-/NO_2^-$) = 1.3 V,[78] resulting in driving forces of approximately 0.6 V and for the single-electron reduction, and 0.75 V for the two-electron reduction of $ONOO^-$. This would at least thermodynamically favour the two- over the single-electron reduction of this biologically devastating anion, thus favouring the production of the benign nitrite, NO_2^-, as opposed to the production of the toxic nitrogen dioxide radical, $NO_2^{\bullet}$.

Supplementary Material

Refer to Web version on PubMed Central for supplementary material.

Acknowledgments

The authors are thankful to the Croatian Ministry of Science (MZOŠ grant: 006-0061247-0009) and to Duke University's CTSA grant 1 UL 1 RR024128-01 from NCRR/NIH for their financial support.

References

1. Lahaye D, Muthukumaran K, Hung CH, Gryko D, Reboucas JS, Spasojevic I, Batinic-Haberle I, Lindsey JS. Bioorganic & Medicinal Chemistry. 2007; 15:7066–7086. [PubMed: 17822908]
2. Salvemini D, Riley DP, Cuzzocrea S. Nature Reviews Drug Discovery. 2002; 1:367–374.
3. Szabó C, Ischiropoulos H, Radi R. Nature Reviews Drug Discovery. 2007; 6:662–680.
4. Wood PM. Biochemical Journal. 1988; 253:287–289. [PubMed: 2844170]
5. Sawyer DT, Valentine JS. Accounts of Chemical Research. 1981; 14:393–400.
6. Vance CK, Miller AF. Biochemistry. 1998; 37:5518–5527. [PubMed: 9548935]
7. Batinic-Haberle I, Rajic Z, Tovmasyan A, Reboucas JS, Ye X, Leong KW, Dewhirst MW, Vujaskovic Z, Benov L, Spasojevic I. Free Radical Biology and Medicine. 2011; 51:1035–1053. [PubMed: 21616142]

8. Batinić-Haberle I, Rebouças JS, Spasojević I. Antioxid Redox Signal. 2010; 13:877–918. [PubMed: 20095865]
9. Batinic-Haberle, I.; Reboucas, JS.; Benov, L.; Spasojevic, I. Handbook of Porphyrin Science. Kadish, KM.; Smith, KM.; Guillard, R., editors. Vol. 11–15. World Scientific; Singapore: 2011. p. 291-393.
10. Batinić-Haberle I, Spasojević I, Tse HM, Tovmasyan A, Rajić Z, Clair DKS, Vujasković Ž, Dewhirst MW, Piganelli JD. Amino Acids. 2012; 42:95–113. [PubMed: 20473774]
11. Spasojević I, Chen Y, Noel TJ, Yu Y, Cole MP, Zhang L, Zhao Y, StClair DK, Batinić-Haberle I. Free Radical Biology and Medicine. 2007; 42:1193–1200. [PubMed: 17382200]
12. Batinić-Haberle I, Spasojević I, Stevens RD, Bondurant B, Okado-Matsumoto A, Fridovich I, Vujaković Ž, Dewhirst MW. Dalton Transactions. 2006:617–624. [PubMed: 16402149]
13. Spasojević I, Batinić-Haberle I, Rebouças JS, Idemori YM, Fridovich I. Journal of Biological Chemistry. 2003; 278:6831–6837. [PubMed: 12475974]
14. Batinić-Haberle I, Spasojević I, Hambright P, Benov L, Crumbliss AL, Fridovich I. Inorganic Chemistry. 1999; 38:4011–4022.
15. Saba H, Batinic-Haberle I, Munusamy S, Mitchell T, Lichti C, Megyesi J, MacMillan-Crow LA. Free Radical Biology and Medicine. 2007; 42:1571–1578. [PubMed: 17448904]
16. Miriyala S, Spasojevic I, Tovmasyan A, Salvemini D, Vujaskovic Z, StClair D, Batinic-Haberle I. Biochimica et Biophysica Acta (BBA) - Molecular Basis of Disease. 2012; 1822:794–814.
17. Tovmasyan A, Sheng H, Weitner T, Arulpragasam A, Lu M, Warner DS, Vujaskovic Z, Spasojevic I, Batinic-Haberle I. Medical Principles and Practice. 2013; 22:103–130. [PubMed: 23075911]
18. Rebouças JS, DeFreitas-Silva G, Spasojevic I, Idemori YM, Benov L, Batinic-Haberle I. Free Radical Biology and Medicine. 2008; 45:201–210. [PubMed: 18457677]
19. Zhao Y, Chaiswing L, Velez JM, Batinic-Haberle I, Colburn NH, Oberley TD, StClair DK. Cancer Research. 2005; 65:3745–3750. [PubMed: 15867370]
20. Kos I, Benov L, Spasojevic I, Reboucas JS, Batinic-Haberle I. Journal of Medicinal Chemistry. 2009; 52:7868–7872. [PubMed: 19954250]
21. Lee J, Hunt JA, Groves JT. Journal of the American Chemical Society. 1998; 120:6053–6061.
22. Ferrer-Sueta G, Vitturi D, Batinic-Haberle I, Fridovich I, Goldstein S, Czapski G, Radi R. Journal of Biological Chemistry. 2003; 278:27432–27438. [PubMed: 12700236]
23. Ferrer-Sueta G, Batinić-Haberle I, Spasojević I, Fridovich I, Radi R. Chemical Research in Toxicology. 1999; 12:442–449. [PubMed: 10328755]
24. Batinić-Haberle I, Spasojević I, Stevens RD, Hambright P, Fridovich I. Dalton Transactions. 2002:2689–2696.
25. Spasojević I, Batinić-Haberle I, Fridovich I. Nitric Oxide - Biology and Chemistry. 2000; 4:526–533.
26. Radi R. Chemical Research in Toxicology. 1998; 11:720–721. [PubMed: 9671533]
27. Ferrer-Sueta G, Hannibal L, Batinic-Haberle I, Radi R. Free Radical Biology and Medicine. 2006; 41:503–512. [PubMed: 16843831]
28. Nadezhdin AD, Dunford HB. Canadian Journal of Chemistry. 1979; 57:3017–3022.
29. Tovmasyan A, Weitner T, Roberts E, Vujaskovic Z, Leong KW, Spasojevic I, Batinic-Haberle I. Antioxid Redox Signal. 2013 submitted.
30. Jaramillo MC, Briehl MM, Crapo JD, Batinic-Haberle I, Tome ME. Antioxid Redox Signal. 2013 submitted.
31. Budimir A, Kalmar J, Fabian I, Lente G, Banyai I, Batinic-Haberle I, Birus M. Dalton Transactions. 2010; 39:4405–4410. [PubMed: 20422097]
32. Weitner T, Budimir A, Kos I, Batinic-Haberle I, Birus M. Dalton Transactions. 2010; 39:11568–11576. [PubMed: 21052598]
33. Harriman A, Porter G. Faraday Transactions. 1979:1532–1542.
34. Harriman A. Dalton Transactions. 1984:141–146.

35. Tovmasyan A, Weitner T, Sheng H, Lu M, Rajic Z, Warner DS, Spasojevic I, Reboucas JS, Benov L, Batinic-Haberle I. Inorganic Chemistry. 2013; 52:5677–5691. [PubMed: 23646875]
36. Groves JT, Lee J, Marla SS. Journal of the American Chemical Society. 1997; 119:6269–6273.
37. De Angelis F, Jin N, Car R, Groves JT. Inorg Chem. 2006; 45:4268–4276. [PubMed: 16676990]
38. Lahaye D, Groves JT. Journal of Inorganic Biochemistry. 2007; 101:1786–1797. [PubMed: 17825916]
39. Jin N, Bourassa JL, Tizio SC, Groves JT. Angewandte Chemie International Edition. 2000; 39:3849–3851.
40. Adams, R. Electrochemistry at Solid Electrodes. Marcel Dekker; New York: 1969.
41. Yin H, Ma Q, Zhou Y, Ai S, Zhu L. Electrochimica Acta. 2010; 55:7102–7108.
42. Konopka SJ, McDuffie B. Analytical Chemistry. 1970; 42:1741–1746.
43. Rudolph, M. 4.0. ElchSoft; Am Kötschauer Weg 7, 99510 Kleinromstedt, Germany: 2006.
44. Nicholson RS, Shain I. Analytical Chemistry. 1964; 36:706–723.
45. Paul HJ, Leddy J. Analytical Chemistry. 1995; 67:1661–1668.
46. Evans DH, O'Connell KM, Petersen RA, Kelly MJ. Journal of Chemical Education. 1983; 60:290.
47. Nicholson RS. Analytical Chemistry. 1965; 37:1351–1955.
48. Bard, AJ.; Faulkner, LR. Electrochemical methods - Fundamentals and Applications. John Wiley & Sons, Inc; New York: 2001.
49. Budimir A, Šmuc T, Weitner T, Batinic-Haberle I, Biruš M. Journal of Coordination Chemistry. 2010; 63:2750–2765.
50. Laviron E. Journal of Electroanalytical Chemistry. 1983; 146:1–13.
51. Laviron E. Journal of Electroanalytical Chemistry. 1983; 146:15–36.
52. Laviron E. Journal of Electroanalytical Chemistry. 1981; 130:23–29.
53. Laviron E. Journal of Electroanalytical Chemistry. 1981; 124:1–7.
54. Laviron E. Journal of Electroanalytical Chemistry. 1981; 124:9–17.
55. Bates, RG. Treatise on Analytical Chemistry, Part I. 2. Kolthoff, IM.; Elving, PJ., editors. Vol. 1. Wiley; New York: 1978. p. 793
56. Trassati S. Pure and Applied Chemistry. 1986; 58:955–966.
57. Fang Z, Zhang H, Zhang P, Huang S, Guo L, Hu G. Acta Metallurgica Sinica. 1996; 9:189–192.
58. Anson FC, Osteryoung RA. Journal of Chemical Education. 1983; 60:293–296.
59. Sucheta A, Rusling JF. Electroanalysis. 1991; 3:735–739.
60. Einstein A. Annalen der Physik. 1905; 322:549–560.
61. Jones G, Christian SM. Journal of the American Chemical Society. 1937; 59:484–486.
62. Sutherland W. Philosophical Magazine Series 6. 1905; 9:781–785.
63. Lide, DR., editor. CRC Handbook of Chemistry and Physics. CRC Press; 2005.
64. Muller P. Pure and Applied Chemistry. 1994; 66:1077–1184.
65. Dean, JA. Lange's Handbook of Chemistry. McGraw-Hill, Inc; New York: 1999.
66. Gray GW, Spence JT. Inorganic Chemistry. 1971; 10:2751–2755.
67. Ball EG. Journal of Biological Chemistry. 1937; 118:219–239.
68. Saveant JM. Energy & Environmental Science. 2012; 5:7718–7731.
69. Atkins, PW. Physical Chemistry. Oxford University Press; Oxford: 1998.
70. Kos I, Reboucas JS, DeFreitas-Silva G, Salvemini D, Vujaskovic Z, Dewhirst MW, Spasojevic I, Batinic-Haberle I. Free Radical Biology and Medicine. 2009; 47:72–78. [PubMed: 19361553]
71. Abe T. The Journal of Physical Chemistry. 1986; 90:713–715.
72. Bashford D, Case DA. Annual Review of Physical Chemistry. 2000; 51:129–152.
73. Bucher M, Porter TL. The Journal of Physical Chemistry. 1986; 90:3406–3411.
74. Koneshan S, Rasaiah JC, Lynden-Bell RM, Lee SH. The Journal of Physical Chemistry B. 1998; 102:4193–4204.

75. Spasojevic I, Kos I, Benov LT, Rajic Z, Fels D, Dedeugd C, Ye X, Vujaskovic Z, Reboucas JS, Leong KW, Dewhirst MW, Batinic-Haberle I. Free Radical Research. 2010; 45:188–200. [PubMed: 20942564]

76. Evans DH. Journal of Electroanalytical Chemistry and Interfacial Electrochemistry. 1989; 258:451–456.

77. Valez V, Cassina A, Batinic-Haberle I, Kalyanaraman B, Ferrer-Sueta G, Radi R. Archives of Biochemistry and Biophysics. 2013; 529:45–54. [PubMed: 23142682]

78. Koppenol WH. Free Radical Biology and Medicine. 1998; 25:385–391. [PubMed: 9741577]

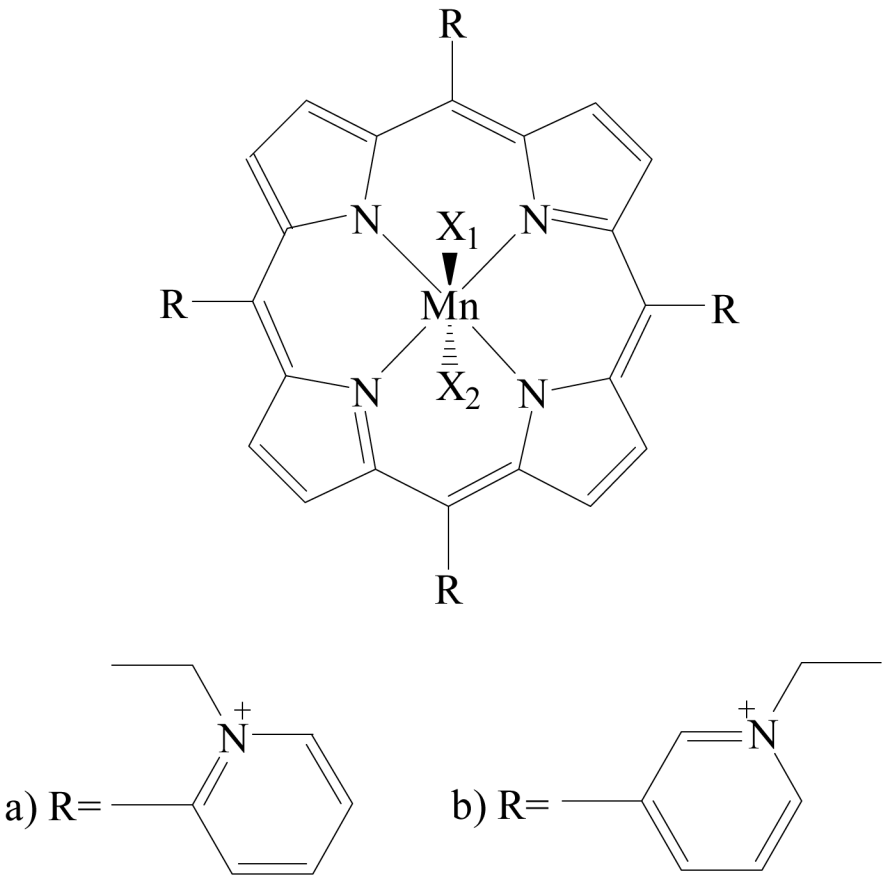

Figure 1.

a) Manganese *ortho* tetrakis(*N*-ethylpyridinium-2-yl)porphyrin ≡ MnTE-2-PyP, b) Manganese *meta* tetrakis(*N*-ethylpyridinium-3-yl)porphyrin ≡ MnTE-3-PyP. X_1 and X_2 stand for the aqua, hydroxo, or/and oxo ligand(s), with X_2 not necessarily included. Charges are omitted throughout the text for clarity.

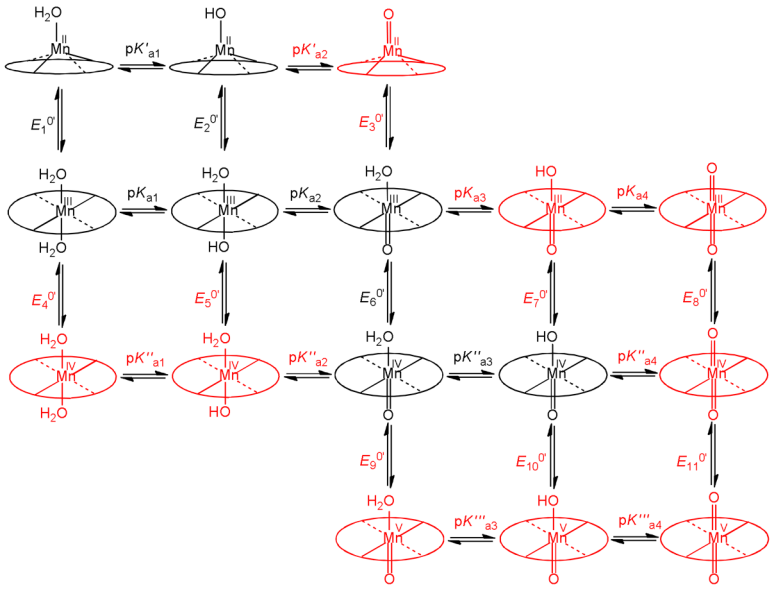

Figure 2.
Equilibria describing the observed behaviour of MnPs in aqueous solutions.[32] The experimentally unavailable species and related thermodynamic parameters are coloured red.

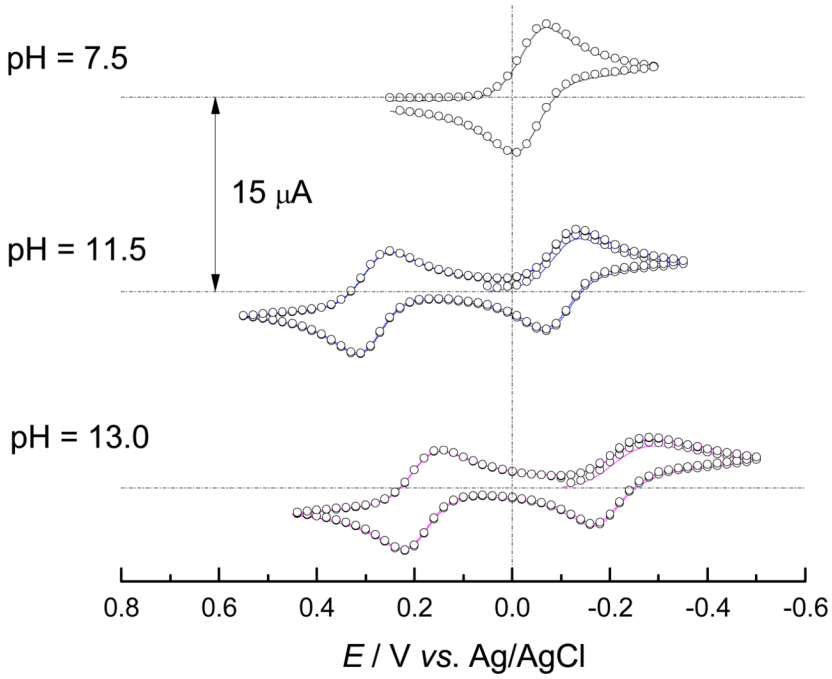

Figure 3.

Dependence of cyclic voltammograms of aqueous solutions of MnTE-2-PyP on pH, $\nu = 0.1$ V s^{-1}, [NaCl] = 0.1 M, $\theta = 25$ °C, (○) simulation in DigiElch. Similar behaviour has been reported previously for methyl and butyl analogues, MnTM-2-PyP and MnTnBu-2-PyP.[23, 49] Redox couples shown relate to the $Mn^{IIII}/Mn^{II}P$ (right cycle) and the Mn^{IV}/Mn^{III} couples (left cycle).

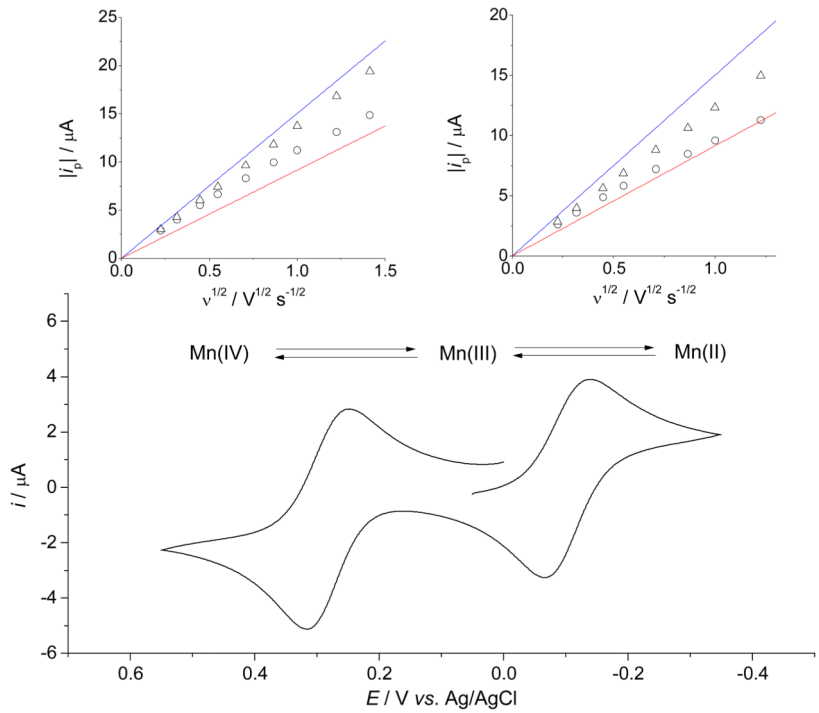

Figure 4.

Cyclic voltammogram of 0.65 mM aqueous solution of MnTE-2-PyP, pH = 11.3, [CAPS] = 50 mM, [NaCl] = 0.1 M, $\nu = 0.1$ V s^{-1}, $\theta = 25$ °C. Inset left: Dependence of $|i_p|$ on $\nu^{1/2}$ for the $Mn^{IV}P/Mn^{III}P$ redox transition: i_{pc} (○), i_{pa} (△), Randles-Ševčik equation for the reversible electron transfer (——), peak-current equation for the irreversible electron transfer, α = 0.3 (——). Inset right: Dependence of $|i_p|$ on $\nu^{1/2}$ for the $Mn^{III}P/Mn^{II}P$ redox transition: i_{pc} (○), i_{pa} (△), Randles-Ševčik equation for the reversible electron transfer (——), peak-current equation for the irreversible electron transfer, α = 0.3 (——). The value of D_{app} obtained by chronocoulometry at the same pH (Table 2) was used for calculation.

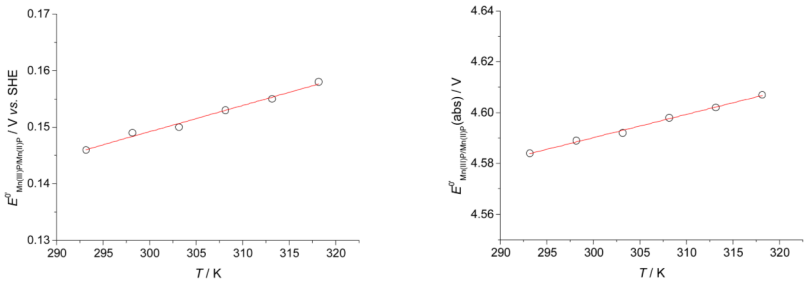

Figure 5.

The temperature dependence of the formal reduction potential (left, $E^{0\prime}$ *vs*. SHE) and the absolute reduction potential (right, $E^{0\prime}$ (abs)) of $Mn^{III}P/Mn^{II}P$ redox couple of MnTE-2-PyP: [MnTE-2-PyP] = 0.65 mM, pH = 7.5, [NaH_2PO_4] = 50 mM, [NaCl] = 0.1 M.

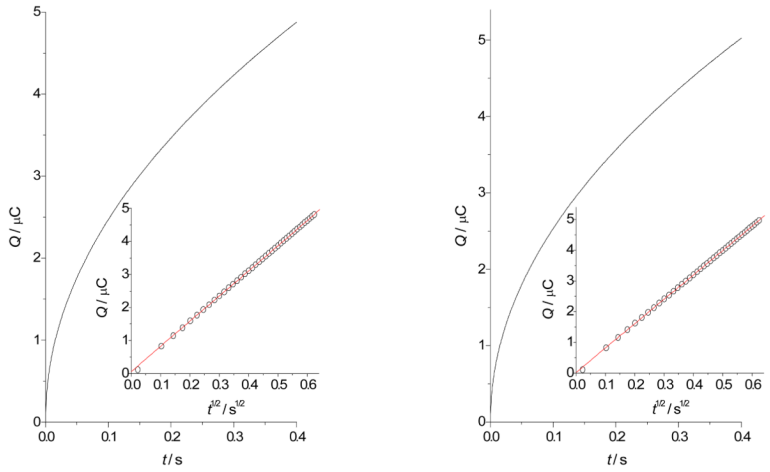

Figure 6.

Chronocoulometry of MnP complexes in aqueous solutions, left: [MnTE-2-PyP] = 0.54 mM, pH = 7.5, [NaH_2PO_4] = 50 mM, [NaCl] = 0.1 M, θ = 25 °C, E_1 = 0.2 V, E_2 = −0.35 V, t_{max} = 0.4 s. Inset left: Anson plot of the observed dependence of the charge Q *vs.* $t^{1/2}$, right: [MnTE-3-PyP] = 0.52 mM, pH = 12.3, [Na_2HPO_4] = 50 mM, [NaCl] = 0.1 M, θ = 25 °C, E_1 = 0 V, E_2 = −0.55 V, t_{max} = 0.4 s. Inset right: Anson plot of the observed dependence of the charge Q *vs.* $t^{1/2}$.

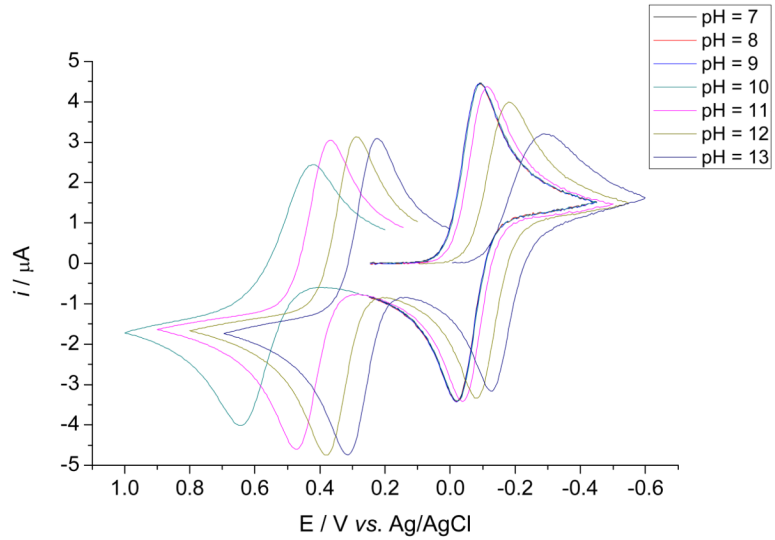

Figure 7.
Simulation of the electrochemical behaviour of a 0.5 mM solution of MnTE-2-PyP in the range of pH values form 7 to 13.

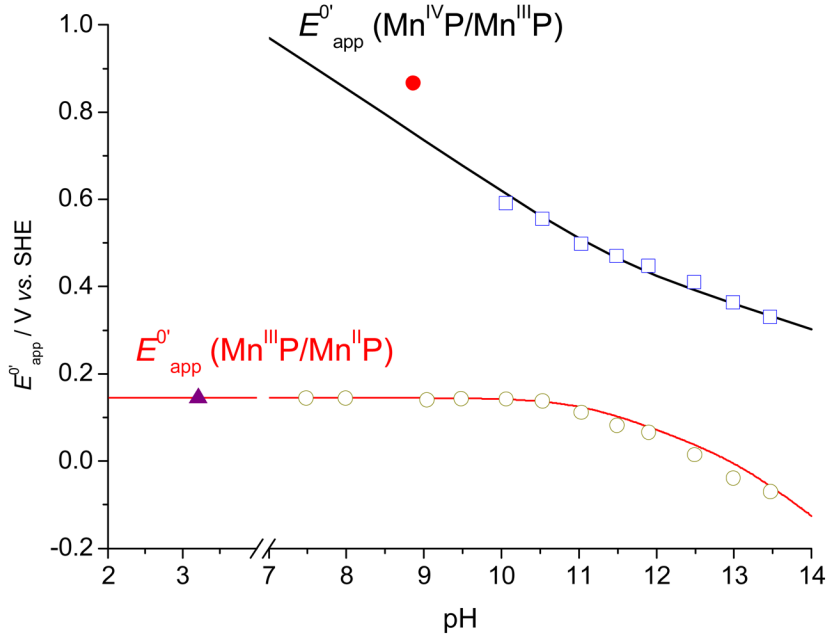

Figure 8.

Comparison of the pH-dependent apparent formal reduction potentials, $E^{0\prime}_{app}$, of the $Mn^{III}P/Mn^{II}P$ and $Mn^{IV}P/Mn^{III}P$ redox couples of MnTE-2-PyP, simulated by eqs. (5) and (8) with various experimental values: (●) oxidation of $Mn^{III}P$ with octacyanomolybdate (ref. 32), (□) cyclic voltammetry of the $Mn^{IV}P/Mn^{III}P$ redox couple (Table S7), (▲) reduction of $Mn^{III}P$ with ascorbate (ref. 32) and (○) cyclic voltammetry of the $Mn^{III}P/Mn^{II}P$ redox couple (Table S7).

Table 1

The thermodynamic parameters of the electroreduction of $Mn^{III}P$ complexes calculated from temperature dependencies of the formal reduction potentials ($E^{0\prime}$ *vs*. SHE) and the absolute reduction potentials ($E^{0\prime}$ (abs)): pH = 7.5, [NaH_2PO_4] = 50 mM, [NaCl] = 0.1 M.

MnP	$\Delta H^{0\prime} \pm \sigma$/kJ mol^{-1}	$\Delta S^{0\prime} \pm \sigma$/J K^{-1} mol^{-1}	$\Delta H^{0\prime}$ (abs) $\pm \sigma$/kJ mol^{-1}	$\Delta S^{0\prime}$ (abs) $\pm \sigma$/J K^{-1} mol^{-1}
MnTE-2-PyP	−29 ± 1	48 ± 3	−469 ± 2	88 ± 7
MnTE-3-PyP	−29 ± 6	106 ± 19	−468 ± 6	145 ± 12

Table 2

The results of chronocoulometric measurement of the electroreduction of Mn^{III}TE-2-PyP and Mn^{III}TE-3-PyP, [NaCl] = 0.1 M, θ = 25 °C.

MnP	pH	$(D_{app} \pm \sigma)/10^{-6}$ cm^2 s^{-1}	$(r_{app} \pm \sigma)$/Å
MnTE-2-PyP	7.5	2.35 ± 0.05	10.3 ± 0.2
	11.3	2.16 ± 0.05	11.2 ± 0.3
	13.0	1.85 ± 0.04	13.1 ± 0.3
MnTE-3-PyP	7.5	2.15 ± 0.05	11.3 ± 0.3
	12.3	2.00 ± 0.05	12.1 ± 0.3
	13.2	1.78 ± 0.04	13.6 ± 0.3

Table 3

Electrochemical parameters for the reduction of the experimentally accessible species of MnP complexes, [NaCl] = 0.1 M, θ = 25 °C. Values of the deprotonation constants were taken from ref. 32: pK'_{a1} = 11.75, pK_{a1} = 10.89, pK_{a2} = 11.62, pK''_{a3} = 11.14 for MnTE-2-PyP and pK'_{a1} = 12.04, pK_{a1} = 11.57, pK_{a2} = 12.70 and pK''_{a3} = 11.99 for MnTE-3-PyP. As previously in Figures 7, 8, S11 and S12, the experimentally unavailable deprotonation constants were taken to be at least one pH unit beyond the studied pH range, *i.e.* pK'_{a2} = 14, pK_{a3} = 14, pK_{a4} = 15, pK''_{a1} = 5, pK''_{a2} = 6, pK''_{a4} = 14.

MnP	couple	index	$E_i^{0\prime}$/V *vs.* SHE*	$k_i^0/10^{-2}$ cm s^{-1}	α_i
MnTE-2-PyP	MnIIIP/MnIIP	1	0.145	0.3	0.4
		2	0.094	0.7	0.3
		3	≤ −0.046	≤ 0.3	0.3
	MnIVP/MnIIIP	5	≥ 0.812	1.0	0.3
		6	0.470	1.3	0.3
		7	≤ 0.301	≤ 1.6	0.4
MnTE-3-PyP	MnIIIP/MnIIP	1	−0.020	0.4	0.4
		2	−0.045	0.8	0.3
		3	≤ −0.121	≤ 0.3	0.3
	MnIVP/MnIIIP	5	≥ 0.779	1.0	0.3
		6	0.390	1.3	0.3
		7	≤ 0.271	≤ 1.4	0.4

*The calculated values differ somewhat from the previously published potentials determined by cyclic voltammetry,[24] due to the differences in methodology and electrode calibration. Yet, importantly, the differences in the formal reduction potentials among the studied members of Mn(III) *N*-alkylpyridylporphyrin series are correct and thus all relationships based on these differences are correct as well.

Table 4

Diffusion coefficients and apparent radii of aqueous cavities of the protonated, mono-deprotonated and di-deprotonated species of $Mn^{III}P$ complexes, [NaCl] = 0.1 M, θ = 25 °C. Values of the deprotonation constants were taken as in Table 3.

MnP	couple	index	$D_O/10^{-6}$ cm^2 s^{-1}	r_O/Å
MnTE-2-PyP	$Mn^{III}P/Mn^{II}P$	1	2.35	10.3
		2	2.24	10.8
		3	≤ 1.83	≥ 13.2
MnTE-3-PyP	$Mn^{III}P/Mn^{II}P$	1	2.15	11.3
		2	2.10	11.6
		3	≤ 1.68	≥ 14.5